IOP Conf. Series: Materials Science and Engineering **388** (2018) 012003 doi:10.1088/1757-899X/388/1/012003

Scatter, Scope and Structures: What fatigue fracture testing of fiber polymer composites is all about

Andreas J Brunner

Empa, Swiss Federal Laboratories for Materials Science and Technology, Laboratory for Mechanical Systems Engineering, Überlandstrasse 129, CH-8600 Dübendorf, Switzerland

andreas.brunner@empa.ch

Abstract. The approach to cyclic fatigue fracture testing of metals and alloys with the data presentation as "Paris-Graph" developed by Paul Paris and co-workers has proven immensely useful for structural engineering. It is, therefore, understandable that the later development of fatigue fracture test methods for fiber-reinforced polymer (FRP) composites followed this route also. However, recently questions have been raised by several researchers that require looking at fatigue fracture of FRP composites in more detail in attempts at using the full potential of this class of materials in structural applications. One of these questions is how the apparent analogy in the shape of the curves between Paris-Graphs of metals, alloys and FRP composites relates to the material specific, physical damage mechanisms. For FRP composites, the investigation of these mechanisms has a long history, but only recently, there seems to be a real advance using sophisticated pattern recognition of acoustic emission waveforms with complementary methods such as multi-physics simulations or high-resolution X-ray computed tomography. Comparing, e.g., crack sizes on the order of tens of micrometers occurring on time-scales of microseconds or less with visually observed delamination propagation, it becomes clear that the data analysis for the Paris-graph is averaging over orders of magnitudes in both, length and time-scales and this inevitably involves some scatter. Another question raised concerns the apparently larger scatter in Paris-Graphs obtained for FRP composites compared to those of metals or alloys. Again, a full understanding of the sources of this scatter has not been reached yet, but likely, the complex morphology and microscopic damage mechanisms of FRP composites play a role. There are further effects from mesoscopic or large-scale fiber bridging in fatigue fracture due to special fiber lay-up used in testing. For structural design with FRP composites, it is not sufficient to select the material performing "best" in the fatigue fracture tests, but it is essential to have safe, reliable, but on the other hand realistic design limits. Scatter in the data and how much of that has to be taken into account first requires understanding the extrinsic (test related) and intrinsic (material related) scatter sources. The concept of a fatigue threshold is also important for fracture-based structural design, since there are indications that threshold values for FRP composites may be quite low.

1. Introduction

A major approach to understanding fatigue fracture in material test coupons goes back to investigations by Paris and coworkers [1] on metals and alloys that finally yielded the so-called "Paris-Graph" of da/dN, the average crack advance per fatigue cycle versus the applied stress intensity K, or the range of applied stress intensity ΔK in a double-logarithmic plot showing essentially a power law

relation with three regions. These are the transition to quasi-static and finally unstable fracture (at "high" values of da/dN and K or ΔK), a roughly linear region in the center (at "intermediate" values of da/dN and K or ΔK), and a so-called threshold region (at "low" values of da/dN and K or ΔK) described in more detail in [2]. Even though the first graph with data published in [1] had not yet adopted the exact form of the plot as described above (the X-axis showing the stress intensity K was plotted on a linear rather than a logarithmic scale), the authors concluded (cite).

> *"On the basis of the experimental data given, it is evident that rates of crack growth-for example, those in 2024-T3 and 7075-T6 skins of aircraft structure-may be computed by the theory presented over a wide range of nominal stress levels and crack sizes. The ramifications of such broad correlation imply an analytic theory of fatigue based on a concept of growth from initial imperfections through which structural life may be predicted."*

Applying this concept to engineering structural design proved to be extremely successful and, therefore, it did not take long before the methodology was applied to other types of materials, and, starting in the 1980ies also to fiber-reinforced polymer-matrix (FRP) composites, see, e.g., [3-8].

The successful application of Paris-plots with the empirical data correlation, and their later refinements, in structural engineering may have, at least in part, contributed to the fact that alternative descriptions of fatigue fracture, e.g., based on the Forman- or Hartman-Schijve equation [9] or similar equations used in the NASGRO® software with its database for fatigue crack growth analysis [10] were discussed much less in literature. Until recently, the application of NASGRO® was limited to metals or metal alloys, essentially with a focus on aerospace materials, e.g., [10-13]. Application of a modified Hartman-Schijve equation to fatigue fracture data of FRP composites was first discussed by [14-15]. This now looks promising for quantification of scatter and for determining conservative design limits FRP structures, at least for fatigue fracture under mode I tensile opening loads, as discussed in detail by [16,17].

Another drawback coming from the success of the empirical engineering approach to fatigue fracture characterization might also be the limited insight into the underlying physical micro-mechanisms obtained so far. For metals and alloys the possible effects of the microstructure on the fatigue fracture behavior are still debated; with a recent paper indicating that there no such effects [18]. Much less is known about the micro-and meso-structural effects on the physical damage mechanisms in fatigue fracture of FRP [19]. In the following sections, selected aspects of the characterization of fatigue fracture in FRP composite materials are discussed with a focus on scatter sources, the scope of respective test procedures and the implications for structural design.

2. Procedures for fatigue fracture testing of fiber-reinforced polymer composites and their scope

The only example of a standard fatigue fracture test method available so far is ASTM D6115 [20] for Mode I Fatigue Delamination Growth Onset of Unidirectional Fiber-Reinforced Polymer Matrix Composites. The scope defines (cite)

> *"This test method determines the number of cycles (N) for the onset of delamination growth based on the opening mode I cyclic strain energy release rate (G), using the Double Cantilever Beam (DCB) specimen ….. This test method applies to constant amplitude, tension-tension fatigue loading of continuous fiber-reinforced composite materials. When this test method is applied to multiple specimens at various G-levels, the results may be shown as a G–N curve …".*

The procedure has been developed for a certain class of FRP composites referring to [21] for details:

> *"This test method is limited to use with composites consisting of unidirectional carbon fiber tape laminates with single-phase polymer matrices. This limited scope reflects the experience gained in round robin testing. This test method may prove useful for other types and classes of composite materials, however, certain interferences have been noted ….".*

These interferences mentioned are among others (cite):

> *"Linear elastic behavior is assumed in the calculation of G used in this test method. This assumption is valid when the zone of damage or nonlinear deformation at the delamination front, or both, is small relative to the smallest specimen dimension, which is typically the specimen thickness for the DCB test. .... Delamination growth may proceed in one of two ways: (1) by a slow stable extension or (2) a run-arrest extension in which the delamination front jumps ahead abruptly. Only the first type of growth is of interest in this test method."*

Specifically with respect to application of the test method on other types of FPR composites, it is noted:

> *"Toughness values measured on unidirectional composites with multiple-phase matrices may vary depending upon the tendency for the delamination to wander between various matrix phases. Brittle matrix composites with tough adhesive interleaves between plies may be particularly sensitive to this phenomenon resulting in two apparent interlaminar fracture toughness values: one associated with a cohesive-type failure within the interleaf and one associated with an adhesive-type failure between the tough polymer film and the more brittle composite matrix. ... Nonunidirectional DCB configurations may experience branching of the delamination away from the midplane through matrix cracks in off-axis plies. If the delamination branches away from the midplane, a pure Mode I fracture may not be achieved as a result of the structural coupling that may exist in the asymmetric sublaminates formed as the delamination grows. In addition, nonunidirectional specimens may experience significant anticlastic bending effects that result in nonuniform delamination growth along the specimen width, particularly affecting the observed initiation values. ... Woven composites may yield significantly greater scatter and unique R curves associated with varying toughness within and away from interlaminar resin pockets as the delamination grows. Composites with significant strength or toughness through the laminate thickness, such as composites with metal matrices or 3D fiber reinforcement, may experience failures of the beam arms rather than the intended interlaminar failures."*

The procedure described in [20] is mainly intended for quantification of the effects of materials or processing variables as well as effects of environmental variables, for quantitative comparison of different FRP composites, but may also serve (cite)

> *"To develop criteria for avoiding the onset of delamination growth under fatigue loading for composite damage tolerance and durability analyses."*

These texts in "Scope" and "Significance and Use" of the ASTM Standard Test Methods for fracture of FRP composites are fairly general and, e.g., do not specify in detail how to develop the failure criteria for damage tolerance or durability analyses. The subject of structural design of composites is covered in more detail in [22]. In the earlier version [23] none of the ASTM fracture or fatigue fracture test methods are explicitly referenced, indicating that the direct use of the fracture mechanics test data in design may possibly require more research before becoming formalized in standards and guidelines.

2.1. Developments toward standard fatigue fracture test procedures for FRP composites

The development of test procedures for quasi-static of cyclic fatigue fracture of FRP composites has been reviewed in detail [24-27]. Currently, there are standard test procedures for quasi-static fracture of FRP composites under three types of loads, so-called Mode I with tensile opening load [21,28,29], Mode II in plane shear [30,31] and for various combinations of Mode I and Mode II [32] and one standard test [20] for fatigue delamination onset. Experimental research and activities in fracture mechanics test groups has explored the applicability of the respective quasi-static set-ups for cyclic fatigue facture testing under Mode I [33-34], Mode II [35,36], and Mixed Mode I/II [15,37,38].

Even though Paris-type graphs can be generated by all these draft procedures data analysis revealed certain limitations, e.g., relatively poor reproducibility [39-41] requiring large safety margins for design. There are also indications that the so-called threshold values that could be used to define design limits are fairly low, see Figure 1 and [34,42]. The straight line in Fig. 1 right indicates an

estimated threshold at 10^{-7} mm/cycle (equivalent to 10^{-10} m/cycle defined as da/dN for an operational threshold in [2]) around 40 J/m^2, assuming that (1) linear extrapolation of the data is justified and (2) scatter in the visual data is not accounted for. If scatter is taken into account, e.g., by taking twice or three-times the standard deviation, the conservative value (design threshold) would be even lower. It can be noted that the data plotted without smoothing seem to indicate an incipient threshold of roughly 60-70 J/m^2 around 10^{-6} mm/cycle. Possibly, this cloud of data points represents scatter due to limited resolution of the load and displacement measurements, respectively, used in the data analysis.

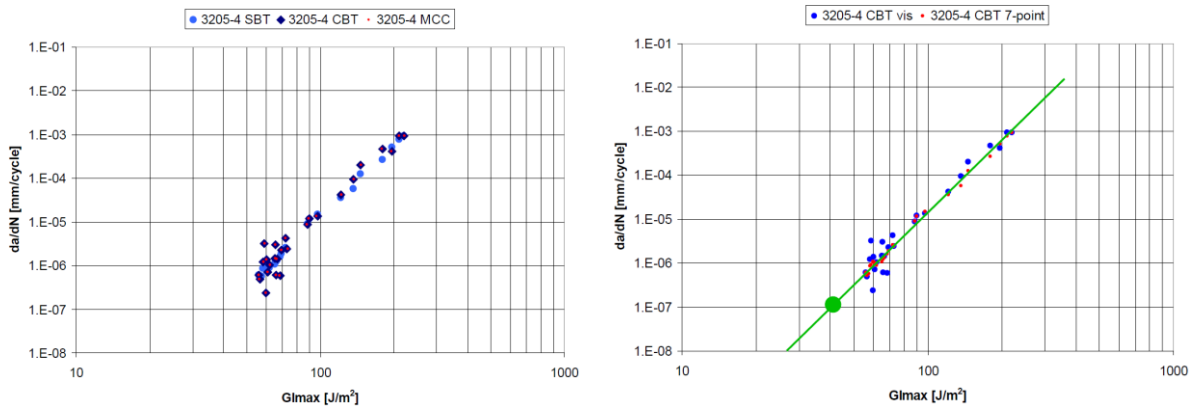

Figure 1. Paris-graph of Mode fatigue fracture data for one type of CFRP (carbon fiber G30-500 / R5259 type epoxy) showing (left) a comparison between different data analysis methods for visually observed delamination lengths (SBT = simple beam theory, CBT = corrected beam theory, MMC = modified compliance calibration) and (right) the data from the CBT-method smoothed with a 7-point polynomial according to [2], the straight green line drawn by eye estimates the da/dN for different applied G_{Imax} values, the green dot indicates the operational threshold $G_{Imax\text{-}thr}$ defined by [2] at 10^{-10} m/cycle.

However, there are recent investigations that point toward intrinsic problems with the cyclic fatigue fracture testing approaches based on the standard quasi-static tests and specifically the choice of the proper X-axis parameter for the data presentation. These issues are briefly summarized in the section below.

2.2. A brief discussion on data analysis and presentation

Since the data presentation for metals or metal alloys based on the double logarithmic da/dN versus K or ΔK graph by Paris et al. [1] was directly applied to FRP composites, the first publications showed da/dN versus ΔK, e.g., the graphs in [5]. Later publications changed the X-axis to either G_{max} or ΔG for the different fracture modes, e.g., the graphs in [39,40,43], since the stress intensity K is experimentally not well defined in FRP composites even though the theory yields (apparently) accurate expressions. As argued in recent publications, e.g., [44,45] replacing K or ΔK by G or ΔG in the Paris-graph does not properly present the fatigue fracture damage in order to predict the behavior of FRP composite structures and equations with "square-root-G" terms are proposed as proper similitude parameter. Rans et al. [44 hence conclude (cite)

> *"Finally, it may be argued that in adopting a Paris relation to fit experimental delamination growth data, the selection of the independent variable for fitting the data is arbitrary. It is merely an exercise in correlating experimental data. This, however, should not be the case. Applying a Paris relation is done not simply to curve fit experimental data, but to attempt to capture the material behaviour based on some basis for similitude. Indeed, numerous bases of similitude could be selected; however, for understanding fracture mechanisms, it is convenient to divide these mechanisms on the basis of cyclic (ΔK, ΔG = (√G_{max} - √G_{min})^2) and monotonic (K_{max}, G_{max}) loading effects."*

Besides that, fatigue fracture data presented in literature often show a fairly large scatter in da/dN for a given value of the X-axis parameter (be it G_{max}, ΔG or a square-root G-type quantity). In the Paris-graph, scatter of one order of magnitude in da/dN is not uncommon (see, e.g., [39,40]) and this results in large safety margins that have to be included structural design noted above. Of course, this will limit the applicability of FRP composite materials in light-weight structures. The sources of scatter that have been identified so far are discussed in more detail later.

This brief summary of the current state suggests two main directions for future testing and design development: One is to improve the understanding of the microscopic damage mechanisms and their potential effects on scatter in the data in a rather long-term perspective (see, e.g., [19] for a first approach on that) and the other in drafting test procedures considering the identified sources of scatter and choosing the proper similitude parameter for data presentation. This can, e.g., be based on the Hartman-Schijve equation noted above or variations of that, essentially involving a dependence of the delamination rate da/dN on a "square-root-G" quantity as similitude parameter (see, e.g., [15,16] for more details). There is a perspective that the Hartman-Schijve equation will allow for obtaining a master curve for FRP structural design simultaneously with estimating safe design limits, at least for Mode I fatigue fracture [16]. Selected aspects of FRP structural design and of the scatter sources in fatigue fracture testing of FRP laminates are discussed next.

3. A note on fracture mechanics based structural design approaches for FRP composites

Even though in most designs of composite structures or elements to date interlaminar fracture or fatigue fracture data are not considered yet, the methodology for a fracture mechanics based design has been outlined almost twenty years ago [46]. In the abstract, the author notes (cite)

> *"In laminated composite structures, interlaminar failures or delaminations have continued to be a predominant life-limiting failure mode. The main concern for designers has focused on the damage tolerance of structures in the presence of delamination damage from impact events. The design approach has been to utilize existing stress/strain-based design criteria to design the part, then to impact the part consistent with the threat and to take a knock-down in design loads in the presence of damage. However, delaminations also occur during service in areas where high interlaminar stresses are present. These are generally at required discontinuities in the design, such as cut-outs, holes, joints or ply-drops. The application of interlaminar fracture mechanics as a design tool for optimizing these regions is still in its infancy and is adopted by very few original equipment manufacturers. This paper addresses this issue and presents the more recent developments in incorporating interlaminar fracture mechanics into design."*

The methodology described in the paper combines modelling with experimental data as follows (cite)

> *"The framework consists of identifying where cracks will initiate from structural discontinuities or high interlaminar stresses, or identifying likely damage threats. Using FE analysis to model the delamination, values of the strain energy release rate are compared with the interlaminar properties of the composite. An assessment is then made as to whether the delamination will initiate and, if so, how far it will grow until it causes failure in another part of the component. This failure may be another delamination or a structural collapse (e.g. fibre breakage or buckling) resulting in component failure."*

Both cyclic fatigue fracture test types, i.e., fatigue delamination onset [20] and a cyclic fatigue delamination propagation test [39,40] yielding Paris-type data plots can provide the experimental data for this design methodology.

Unfortunately, to date, there are very few published examples applying this concept to FRP composite structures or components. One example is the design and analysis of a rotorhub flexbeam for helicopters [47,48]. The conclusion in [48] states (cite)

> *"Nonlinear-tapered flexbeam laminates were cut from a full-size composite helicopter rotor hub flexbeam and were tested under combined constant axial tension and cyclic bending loads. Two different graphite/glass hybrid configurations were studied. The terminated plies*

were dropped in an overlapping stepwise pattern. All of the specimens failed by delaminations first starting as a crack between the tip of the ply drop group and the adjacent resin region, and growing at the interfaces around the dropped ply toward the thick region of the flexbeam. Delaminations grew with increasing number of cyclic loads, and new delaminations formed at other ply-drop locations. A 2-D finite element model was developed representative of the flexbeam geometry, boundary conditions, and loading. The model was analyzed using two commercially available finite element computer programs, ANSYS and ABAQUS. Delaminations of various lengths were simulated in the analytical model by releasing multipoint constraints (MPCs). Strain energy release rates (G) were calculated using the VCCT using both finite element programs. The calculated peak G values were used with material characterization data to calculate fatigue life curves, for comparison with test data. …. A fracture-mechanics-based methodology was used to relate maximum surface strain to the number of loading cycles at delamination onset for each hybrid specimen type. Good agreement was obtained between tests and analyses. The calculations represent the fatigue life from the opening of the crack at the ply-drop tip until delamination onset, but do not include the cycles necessary to open the crack initially."

One important detail in the example is that the (cite)

"Initial delamination from the resin pocket at the plydrop growing toward the thick region of the flexbeam is dominated by mode II."

Already more than 20 years ago, it had been pointed out that fracture test data from standard tests showed effects from fiber-bridging that do not occur, or at least to a much lesser extent, for FRP components or structures made from the same fiber-matrix system with different lay-up (fiber orientation). For mode I Cantwell and Kausch [49] noted (cite)

"Typical engineering composite structures are rarely unidirectional but contain fibres oriented at large angles to each other. The possibility of fibre nesting occurrence is therefore very limited. … The effect of simply orientating the central plies by a few degrees relative to each other appears to have a significant influence upon the mode of crack propagation. The amount of fibre bridging observed on the fracture surfaces of the failed samples was considerably less than that in evidence on the standard DCB specimen. The influence of even relatively small amounts of fibre bridging on the mode of crack advance is clearly evident."

A similar study for mode II [50] concluded (cite)

"Engineering structures based on composite materials are rarely unidirectional in nature but contain plies orientated at widely differing angles. Previous work … has shown that the interlaminar fracture energy at such a ply interface may be significantly different to that associated with an interface between parallel plies. This difference in response is probably associated with fibre bridging, which frequently occurs in unidirectional composites. In this study a number of ENF tests were conducted on samples in which the two centermost plies were offset by four or five degrees. Although this offset angle is comparatively small, it is sufficient to effectively prevent fibre bridging occurring."

This issue has been taken up in recent publications again, pointing out that in quasistatic and cyclic fatigue fracture tests under Mode I tensile opening loads, fiber bridging will inevitably occur and affect the resulting test data [16,17].

Fiber bridging is intrinsic to unidirectional laminate lay-up [51] which is specified as test material in the quasi-static fracture mechanics test standards [21,29]. Since most designs of FRP composites do not use unidirectional fiber lay-up, in the structural material the delamination propagation is much less affected by fiber bridging than in the standard test specimens. The reason that the fracture mechanics design methodology worked well for rotorhub flexbeams likely is that under Mode II in-plane shear loads fiber bridging is not as dominant as under Mode I, even though the Mode II fracture process zone can be of a quite complex shape and comparatively large size which makes the exact determination of the delamination length in the quasi-static and the cyclic fatigue fracture tests difficult [52].

Molent and Forrester [17] recently reviewed the available data on cyclic fatigue growth and residual strength for composite aircraft structures and concluded (cite)

> *"In this paper the growth of some (limited) composite laminate and bonded repair damage types was reviewed and found to broadly conform to the lead crack framework. Thus equations originally derived for metals may have utility for the assessment of the growth of defects in composite structures. One such equation is the Hartman-Schijve variant. With further research (and data) a damage-tolerance approach appears to be feasible and could be used to comply with the 2009 US Federal Aviation Administration (FAA) slow growth approach to certifying composite, adhesively bonded structures and bonded repairs."*

The approaches for testing and data analysis currently under discussion [19,41] likely provide a road-map toward this goal.

4. Extrinsic and intrinsic sources of scatter in fatigue fracture of FRP composites and their quantification

Identifying sources of scatter in fracture tests and quantifying the contributions from different sources is important for determining useful fracture mechanics test data [19]. Often, repeatability, i.e., the scatter from testing several, nominally identical specimens in one single laboratory, ideally by the same operator and the same test set-up is quoted as an average value with related standard deviation. Similarly, reproducibility, i.e., performing the same test on identical specimens at different laboratories, by different operators and possibly different test set-ups, yields again an average value with a standard deviation. The main purpose of a standard test procedure is to minimize the scatter in both, repeatability and reproducibility. For that, the sources of scatter have to be identified and the test procedure requirements defined sufficiently. Following [19], scatter sources are classified as extrinsic and intrinsic, respectively. Intrinsic scatter is essentially coming from the (unavoidable) variability in microscopic, mesoscopic and macroscopic properties of the FRP laminates. These typically reflect the manufacture and processing of the laminate and the test specimens prepared from that. Ideally, the specification of the specimen manufacture and processing should yield samples that show the full range of manufacturing and processing variability of the FRP composites structures or components. Extrinsic scatter is then attributed to, e.g., test setup, testing parameters, and possibly data analysis. This is discussed in more detail below.

4.1. Extrinsic sources of scatter

A first source of extrinsic scatter has been identified in the round robin tests reported by Stelzer et al. [39,40] coming from the resolution of the load cell. Typical loads measured in the fracture and fatigue fracture tests amount to 100-200 N and these values often drop to a few tens of N under displacement control. Therefore, the load cell measurement range shall be 250 N or less, or else a proper load signal calibration has to be performed in that range. Similarly, the displacement measurement may also be affected by the resolution of the measurement device. A recent study [53] illustrates this by providing estimates of the uncertainty in measurements of fracture toughness, however not on FRP composites, taking into account several experimental parameters. The so-called "human factor", i.e., the experience of the operator in setting-up and performing the tests [54] as well as acquiring the data, e.g., the visual measurement of the delamination length, also plays an important and often underestimated role. Specimen manufacturing, processing and preparation (often also done by humans, sometimes supported by robots or computer-controlled equipment that, however, also have limitations in their accuracy) also yields scatter, e.g., by variation in fiber orientation during lay-up resulting in fiber misalignment or waviness, variation of plate thickness and specimen width (some standards set limits on variation in specimen dimensions, e.g., [21,29], and quality of cutting from the plate. Variation in fiber orientation and specimen geometry or size may affect the compliance of the test specimens which in turn affects the test data [51]. Even if variations in specimen size are limited by specifying tolerances in the test standards or guidelines and unsuitable specimens are excluded; some *intrinsic* material variability and hence scatter will remain. Finally, the operator experience or human factor

also comes into play in the analysis, e.g., when determining the non-linear or 5% change in compliance points for defining the initiation toughness as clearly shown by the example discussed by Davies [55]. This is one motivation for trying to automate the test performance and data analysis as much as possible and to eliminate operator dependent error and scatter sources [56].

The compliance of the test specimens, calculated from machine or test specimen displacement and applied load can be used to calculate the delamination length for quasi-.static or cyclic fatigue fracture under Mode I loading [39,40]. The compliance of the test set-up has to be determined separately and deducted from the compliance calculated from the test machine data. Fig. 2 left shows the specimen compliance as a function of load cycles in fatigue fracture of (carbon-fiber/epoxy type IM7/977-3) calculated in two different ways. The first calculation takes simply the maximum load P_{max} and the maximum displacement δ_{max} (the test was performed under displacement control), i.e., assumes that the respective load-displacement curve can be extrapolated back to zero load and displacement simultaneously (represented by the blue line in Fig. 2). However, if the specimen compliance is calculated as the slope (assumed to be a straight line) between the minimum and maximum values of displacement and load, respectively, the resulting compliance is higher for any given cycle number (red curve in Fig. 2). Therefore, the "effective" compliance of the specimen under cyclic, displacement-controlled fatigue between maximum and minimum displacements (defining the displacement-ratio) is higher than that evaluated from the peak displacements and loads and the same holds for the effective delamination lengths calculated from the compliance, i.e., longer delamination lengths for the analysis based on the larger effective compliance.

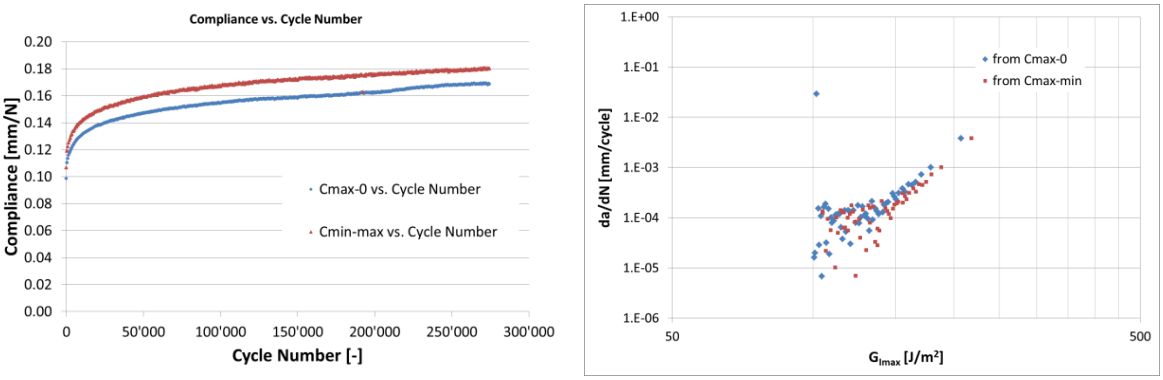

Figure 2: The compliance calculated via two different methods, once from maximum load and displacement (red dots) and once from the difference between maximum and minimum load and displacement (blue dots), respectively (left) and the comparison of the Paris-type graph resulting from delamination lengths calculated with the two compliance methods.

Fig. 2 right shows the resulting Paris-type graph (double-logarithmic da/dN versus G_{Imax}) for the two compliance measurements and the delamination lengths back-calculated from that, respectively. The delamination lengths for the two compliance measurements have been determined using the cubic relation between compliance and delamination length with the equations shown in Appendix 1 of [57] with estimated values of the tensile modulus $E_1$of 150 GPa and shear modulus G13 of 4.9 GPa. The G_{Imax} data have been calculated with the Modified Compliance Calibration Method without applying the load-block and large displacement corrections (Factors F and N according to [29]). It has to be noted that the data sets have been filtered to show data points for a minimum delamination length increase of about 0.1 mm only. Even though the delamination lengths differ due to the different compliance, the Paris-graph data for the two sets, at first sight, agree fairly well. There seems to be a trend to being less conservative and possibly showing slightly larger scatter for data calculated from the compliance based on maximum and minimum values of displacement and load, i.e., for the data yielding higher compliance, compared with those calculated from the maximum values. These trends will, in any case, have to be confirmed and quantified in further analysis comprising more test data.

4.2. Intrinsic sources of scatter

Intrinsic scatter sources have been defined as being material and/or processing related and these have to be taken into account in structural design, as discussed above. One important type of intrinsic scatter that has to be considered, if the data are being used in FRP structural design, i.e., the large-scale fiber bridging due to the unidirectional fiber alignment in the standard fracture test specimens, has already been discussed above. Possible approaches for the quantification of this are discussed in a separate section below.

Manufacturing and processing of FRP composites can yield intrinsic defects such as, e.g., porosity, inclusion of foreign particles, inhomogeneous micro- and meso-scale fiber volume fractions and fiber alignment, local fiber-matrix debonds, etc. [58]. Residual stresses also arise from processing, specifically the cure and post-cure conditions [59], and may interfere with the applied global stresses during testing and thus affect the delamination behavior. Scatter in fiber alignment for a carbon-fiber thermoplastic composite has been quantified by [60]. The fibers in this case lie within about ±3° from the nominal fiber direction with standard deviations between about 0.6° and 1.9°. Wavy fiber plies can also affect the mechanical properties of the laminate as discussed in detail for IM7/8552 [61]. The quantification of intrinsic defects and of their effects on fracture and fatigue fracture behavior requires further investigation for minimizing intrinsic scatter.

5. Accounting for large-scale fiber-bridging in Mode I fatigue fracture of unidirectional fiber-reinforced polymer composites

5.1. Materials approach

Since fiber-bridging is considered to be intrinsic to testing unidirectional FRP composite laminates, the question could be asked whether choosing another laminate lay-up with different fiber orientation might reduce or completely prevent fiber bridging. In early literature on fracture testing, it was recommended to use a lay-up with a slight offset angle (typically 3-5°) for the two plies between which the delamination was propagating in order to reduce fiber-bridging in Mode I and Mode II loading [49,50]. However, the effect of angle-ply lay-ups on fiber bridging in material coupon testing was usually not quantified. Most documented fiber bridging to date is essentially from visual observation or photography, see, e.g., [62-64].

Selected values of G_{IC} and G_{IIC}, respectively, determined from quasi-static fracture testing of angle-ply laminates reported in the literature are summarized in Fig. 3. The data (AS1/3502 [65], AS4/8552 [66], T800H/3631 [67], IM7-G/8552 [68], C12K/R6367 [69], AS4/3501-6 [70] and T300/914C [71]) are plotted as a function of the fiber orientation angle between the two plies between which the delamination initiates or propagates. This angle does not necessarily correspond to the angle between the main delamination direction and the fiber orientation of the adjacent plies, e.g., in ±15° or ±30° lay-ups with delamination propagation in 0° direction which would be shown under 30° and 60°, respectively. Nicholls and Gallagher [65] report average data for selected areas of delamination identified by fractography (described in their paper) and hence their data are labelled as “propagation” values rather than initiation. Sebaey et al. [66] distinguish initiation and propagation, the latter correspond to values from delaminations without jumps to other planes only. Chou et al. [67] also report propagation values for selected delamination areas in addition to initiation values. Some of the authors also provide information on scatter or standard deviation for their average values, but this is not considered in the graphs in Fig. 3.

There is scant data on “small” angles below 10° and it is not clear whether or how data for larger angles can be extrapolated to lower values. For Mode I, the data in Fig. 3 indicate that there is little effect of fiber orientation at delamination initiation (unless precracking has been performed). This is not surprising, since the fiber orientation likely does not affect the resin pocket around the starter film insert. However, delamination propagation after initiation or precracking results in clearly increasing R-curve behavior, i.e., increasing G_{IC} values with increasing delamination length, sometimes noted likely to be due to fiber bridging (from visual observation) in the references. G_{IC} initiation also seems

to increase with increasing difference in angle between the fiber plies adjacent to the delamination. For Mode II, the data tend to show a slight decrease in the G_{IIC} initiation values, if the fiber angle difference is increased, but there are exceptions, e.g., [71]. High propagation values (high compared to G_{IC} initiation) have also been noted for cross-ply (0°/90°) stacked laminates [72,73] that can be considered the extreme case among angle-ply laminates. Multi-directional or quasi-isotropic FRP laminates often yield multiple cracking or crack branching, that, similar to cross-ply might involve mixed mode or inter-laminar and intra-laminar fracture, as discussed, e.g., by [74] and hence is not well suited for determining design values from coupon testing.

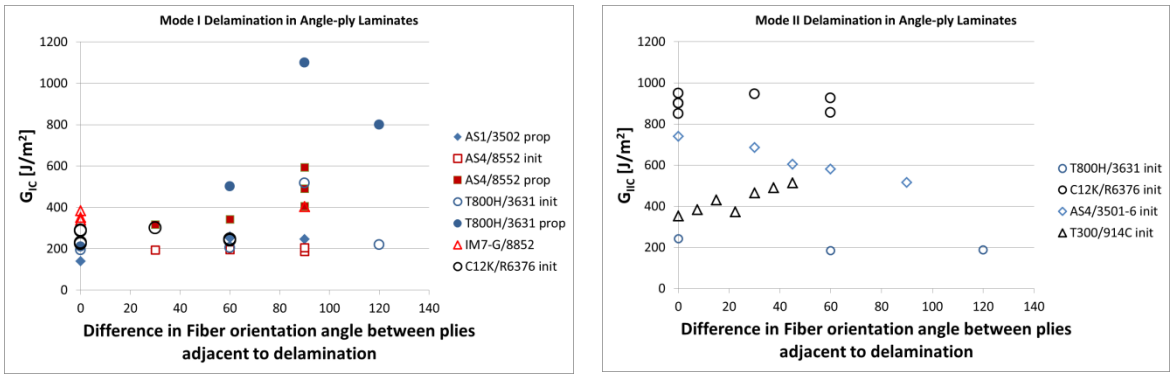

Figure 3. Quasi-static Mode I and Mode II delamination initiation (init) and propagation (prop) values for selected angle-ply CFRP laminates from literature (see text for references and discussion).

5.2. Experimental approaches

Recent publications by the Structural Integrity & Composites Group in Aerospace Engineering at TU Delft provide a perspective for an experimental approach for quantifying the effect of fiber bridging in unidirectional FRP composites subject to cyclic Mode I fatigue loading [41,75,76]. For details, the reader is referred to the referenced literature and the paper presented by Dr. Alderliesten at this symposium [77].

Another, independent approach for accounting for fiber bridging was published by Hojo et al. [78,79]. This method is based on fatigue fracture testing (again Mode I only was considered here) at constant level of G_{max} or ΔG. The data obtained from these experiments can then be extrapolated to short delamination lengths $\Delta a \sim 0$ mm yielding a fatigue fracture curve in the Paris-type graph which is not affected by fiber bridging. While the method proposed by the group at TU Delft likely is more easily implemented in a standard test procedure, the constant-G or constant-ΔG tests may serve as an independent method for validation of the other approach. So far, there is no data available performing both tests on the same material.

5.3. Modelling approaches

There have also been attempts at using modelling or simulation methods to quantify fiber bridging in quasi-static Mode I tests. One example of that is [80], where the author states (cite)

> *"This paper presents a beam model based on a linear traction–separation law that has been shown to be a good approximation to the early stages of fibre bridging. The present model enables the evaluation of accurate propagation GIc values through the fitting of experimental load–displacement curves."*

At this stage, it is not clear whether this or similar modelling approaches could be extended to cyclic Mode I fatigue fracture (private communication from Prof. A.B. de Morais), but it might be worthwhile to explore this in future research.

6. Microscopic damage mechanisms in quasi-static and fatigue fracture and their averaging on macroscopic scales

Due to the morphology of FRP composites, there are several different types of microscopic or mesoscopic damage mechanisms that can be activated by quasistatic or fatigue loads. These are usually noted to be: matrix cracks, fiber-matrix debonding or interface failure, and fiber breaks, see, e.g., [81]. Some authors include (interlaminar) delamination or large matrix cracks as an additional damage mechanism for FRP composites, but as discussed by [82,83], these consist again of a series of smaller size matrix cracks, adding up to larger damage between the ply levels. For more insight into the physical damage mechanisms in FRP, besides identifying the type, also the typical size and time scales are of interest [19]. These issues are briefly discussed here.

One nondestructive monitoring method that is quite sensitive to generation of small defects in many types of materials including in FRP composites is Acoustic Emission (AE), see, e.g., [81,84] for details. The combination of unsupervised AE signal pattern recognition and Multiphysics modelling of wave propagation from model signal sources embedded a FRP composite yielded three AE signal clusters and modelled AE signal parameters attributed to different model sources consistent with matrix cracks, fiber-matrix debonding and fiber breaks [85]. This methodology can be applied to large-scale FRP composite structures, such as wind-rotor blades and yields locations of microscopic damage sources in the structure as well as identification of the damage mechanism type, see, e.g., [86]. However, without suitable damage models, a direct prediction of the life-time of the component from a mapping of locations and type of accumulated microscopic damage, as argued in [87], is not feasible.

In spite of the success of the analysis of AE signals with pattern recognition and source mechanism modelling, this approach does not yield direct quantification of the size or extent of the microscopic damage created by a specific source mechanism. For this, imaging non-destructive test methods, such as X–ray radiography or computed tomography can provide some information on damage location and size. This has been explored in a preliminary analysis of carbon-fiber epoxy composite laminates after quasi-static and cyclic fatigue Mode I fracture testing. One example of a X-ray computed tomography slice taken from a Mode I specimen after quasi-static fracture testing is shown in Fig. 4. There are crack-like features that seem to be oriented parallel to the main delamination. The thickness of this slice (normal to the delamination) is about 3.5 mm, the length of the micro-cracks hence amounts to between about 350 and 1200 μm. The size of the micro-crack features in the thickness direction of the specimen is comparable to the voxel size of about 3 μm or less, and hence, they are difficult to clearly identify. Therefore, a 2-dimensinal Fourier Transform map of the X-ray image slice has been calculated and compared with the same algorithm applied to image slices from unloaded parts of the specimen. The latter do not show the features highlighted by red arrows in the Fourier Transform map in Fig. 4 and also did not yield indications of crack-like features in the X-ray images. This constitutes first evidence, but that will have to be verified by additional investigations, combining more measurements.

It has to be noted that the X-ray imaging by computed micro-tomography discussed above provides first evidence for the damage created in the so-called fracture process zone around the delamination created by the different fracture tests. Even though the quantification of the micro-crack sizes in the fracture process zone can still be debated, it is nevertheless clear that additional fracture surfaces are created in the FRP composites not detectable by the visual or technical observation (e.g., camera or video recording) of the delamination length on the edges of the specimens. On the other hand, this additional damage is reflected in the compliance of the specimens, and hence at least to some extent in the load and displacement measurements. If the fracture or delamination areas from visual observation together with load and displacement values are used to calculate the toughness or delamination resistance, i.e., the G-value, the effective facture surface might be underestimated, resulting in an overestimate for G and possibly also in less accurate estimates of the related scatter.

The currently available data on damage types and sizes are interpreted as follows: The evidence currently available from AE crack or damage sizing or from X-ray computed tomography indicates stochastic micro-crack formation on lengths scales between about 10 μm and about 200 μm. It is

possible, that cracks sizes smaller than 10 μm do occur in FRP composite fracture and that the AE sizing described here reached its limit of sensitivity. X-ray computed micro-tomography with a voxel size around 3 μm poses a similar resolution limit. That the time scale of microscopic fracture events is on the order of microseconds or even less (see, e.g., [87] for details) indicates that the methods for determining delamination lengths currently used in the fracture tests (e.g., visual observation or photography or video recording) do average over several orders of magnitude in time, and, to a lesser extent, also on the length or volumetric scale (e.g., with the requirement to determine the delamination tip with an accuracy of 0.5 mm [21]. The implied averaging over microscopic and short-time events constitutes a potential source of (intrinsic) scatter that is difficult to quantify. The matrix crack sizes determined from the delaminations obtained by the fracture tests described above can be complemented by a study on another microscopic mechanism, namely fiber-matrix debonding discussed below.

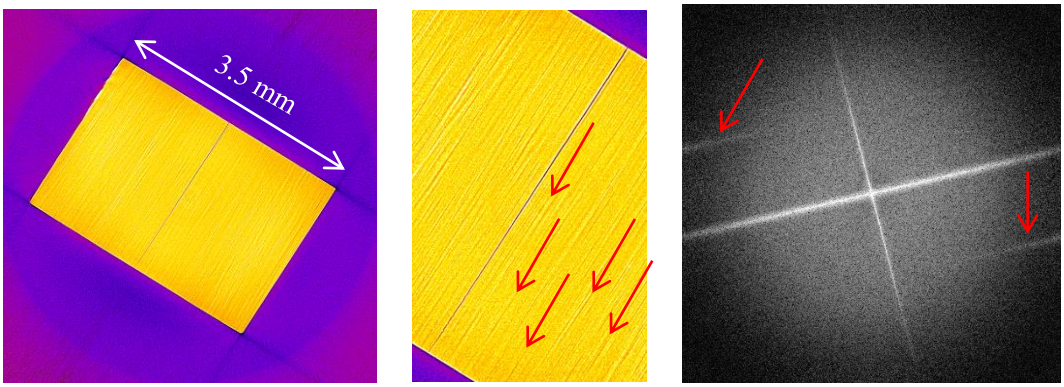

Figure 4: X-ray computed micro-tomography slice (voxel size about 3 μm) of a carbon-fiber epoxy specimen after quasi-static Mode I fracture test (left), a higher magnification of the same slice near the delamination running from the bottom left hand corner to the top right hand corner in the image, selected crack-like features are indicated by red arrows (center) and a 2D Fourier transform of the image (right) showing features (pointed out with red arrows) that are absent from untested specimen parts (see text for details and discussion).

For fiber-matrix debonding, estimates for crack size or debonded surface area can be obtained from micro-mechanical tests. If single fibers (glass or carbon) embedded in an epoxy matrix are subject to quasi-static tensile loading in the so-called single fiber fragmentation test, the fibers will break once a certain stress level is exceeded. Around the location of the fiber break, there occurs also some debonding between fiber and matrix that can be observed under the microscope (Fig. 5). The debond length of course depends on the fiber-matrix adhesion. Increasing the tensile load further after the first fiber break will induce additional fiber breaks until the fiber fragments are too short to be loaded to failure, i.e., reaching saturation. The observed fiber fragment lengths (between about 300 and 400 μm) can be statistically analyzed yielding an average and a width of the distribution [88]. An average debond length for each fiber break of around 80-120 μm can be estimated from the micrographs (Fig. 5), resulting in an average debond area between 1’500 and 2’300 μm^2 for the carbon fibers with a diameter of 6 μm. Similar values of debond length are obtained for glass-fiber epoxy SFFT specimens [88] where fiber diameters are between about 10 and 15 micrometer.

It is known that the SFFT tests do not represent the damage occurring under tensile loads in CFRP since using fiber bundles instead of single fibers indicates that fiber breaks in one fiber affect the occurrence, specifically the location of breaks in adjacent fibers [90]. Even though there are no quantitative data, however, the debond surface area estimates derived from the tests on single fiber specimens likely also apply to multiple fiber specimens. The order of magnitude is of a few tens up to

about 100 micrometers. This range is consistent with the matrix crack sizes (diameters) derived from the AE monitoring of quasi-static fracture tests of FRP composites.

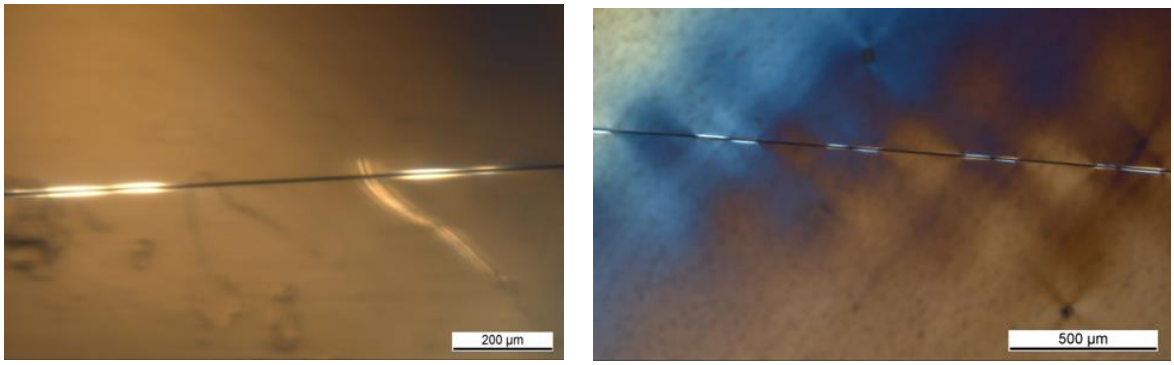

Figure 5. Optical micrographs using polarized light of AS4 carbon fiber breaks after tensile testing single fibers embedded in epoxy matrix, carbon fiber diameter is about 6 µm.

If the applied loading on the embedded fiber is compressive, the so-called single fiber push-in or push-out test yields again debonding between fiber and matrix. The test equipment and set-up is described in detail by Battisti et al. [89]. For carbon fibers embedded in epoxy with a length around 30 micrometers, full debonding was achieved and the fibers effectively pushed-out. With fiber diameters around 6 micrometer and roughly 19 micrometer circumference, the debond area in this case amounts to about 560 µm^2. In analogous experiments with carbon fibers of roughly 300 micrometer length in thicker carbon-fiber epoxy slices, only partial debonding was observed and the fibers failed when increasing the compressive load (unpublished data from the authors' laboratory). Fig. 5 shows examples of this. If the fiber would still debond along the full length of 300 micrometer in the push-in test, the debond area would amount to about 5'600 µm^2 which constitutes an upper limit. Likely, the debond area accumulated up to the point where the fiber fails is less. It has to be noted that Fig. 5 shows a case where the fiber that was pushed in by the indenter is surrounded by a hexagonal close packing of six fibers. The same test was also performed on "isolated" single fibers where the nearest neighbor fiber was at least one fiber diameter (roughly 6 µm) distant from the fiber that was pushed-in. The results for the "isolated" fibers indicate a slightly more compliant behavior and slightly lower failure loads than for the hexagonal closed packed fibers, but no significant difference in failure mode.

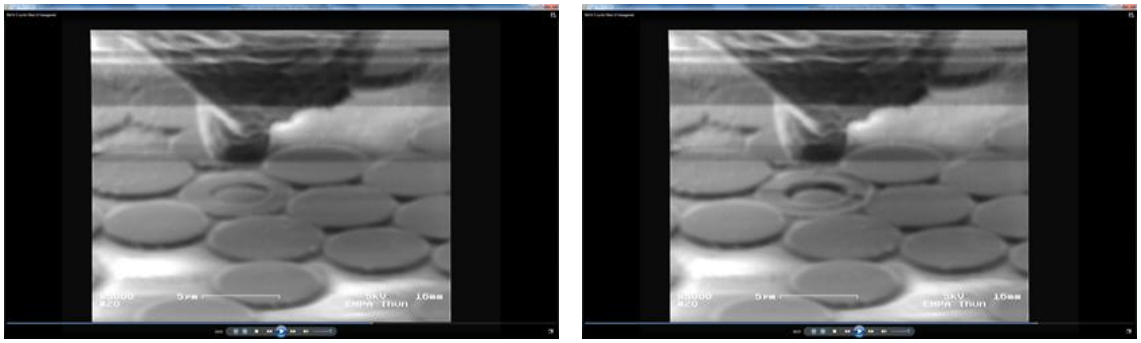

Figure 6. Images from in-situ SEM observation of cyclic push-in loading of a carbon fiber surrounded by a hexagonal group of carbon fibers embedded in a slice of epoxy (about 300 µm thick), first, the indenter tip produces an imprint on the fiber cross-section (left) and finally induces failure (right).

Finally, the question can be asked whether the different types of microscopic damage mechanisms acting in FRP composites and the relevant size or time scales are affected by the micro- or meso-scale

structure or morphology of the materials. Considering the discussion of fiber-matrix debonding above, it could be hypothesized that one factor is the fiber diameter (beside the fiber-matrix adhesion and possible residual stresses from processing [91]) or the average fiber-fiber distance in the composite which is again on the order of a few micrometer or up to a few ten of micrometer at most (in composites with high fiber volume fractions exceeding 60%). The lower size bound of matrix cracks in FRP composites is likely given by the sensitivity of the method used for detection, i.e., of the AE or the X-ray computed micro-tomography. It has to be noted that sub-micron size cracks may not be detected by these methods in all cases. The upper bound estimate, on the other hand, possibly correlates with the typical ply level thickness. Therefore, it could be hypothesized that the micro- and/or meso-scale morphology of the FRP composites, i.e., on scales ranging from a few micrometer up to about 100-150 micrometer, may affect the crack or damage size to some extent, possibly contrary to the case of metals or metal alloys [18]. The evidence so far, however, is too scant to draw firm conclusions and it is definitely worthwhile to investigate this further.

7. Summary and open questions

From the data presented and from the discussion above it can be concluded that (1) there is still no full understanding of the effects that require consideration when testing FRP composite materials under cyclic fatigue loads with the aim of using the data for design limits, but that (2) at least for Mode I tensile opening loads certain extrinsic sources of scatter have been identified (e.g., load cell range used in the test set-up, operator experience) and finally that (3) again at least for Mode I, approaches have been proposed for quantifying the fiber bridging effects intrinsic to the test specimens with unidirectional fiber lay-up for estimating safe design limits for FRP composite components and structures. These approaches may still have to be validated, and possibly optimized, in order to not be too conservative. Likely, the data analysis will remain “empirical”, even when the Paris-type graphs are replaced by master curves based on modified Hartman-Schijve equations [9,15,41]. Getting sufficiently accurate estimates of material- and processing related intrinsic scatter and reducing any extrinsic scatter to a value below that are essential steps towards the application of the data in fracture mechanics based FRP structural design.

The question whether a future damage tolerant design approach for FRP structures can be based on identification and location of micro- and mesoscopic damage events is still open. It is currently not even clear whether the micro- and meso-scale morphology of FRP composites plays a significant role in activating different damage mechanisms. Therefore, attempts at reinforcing the FRP composites with fillers, e.g., nanoparticles or with combinations of particles covering several scales in order to obtain hierarchical FRP composites, e.g., [92], essentially remain empirical and still pose problems for optimization. Therefore, also these issues require further investigation.

The often cited observation that Mode I quasi-static and cyclic fatigue fracture data constitute a conservative limit may also be questioned. To date (to the best knowledge of the author) there is only one example (Fig. 7, left) showing Mode II in-plane shear fatigue fracture data to be more conservative than the corresponding Mode I data. Two tests performed independently by different groups and at different times on the same type of material (AS4/PEEK) agree very well [37,93]. Another question is the behavior of fatigue fracture data obtained under different modes (Mode I tensile opening, Mode II in-plane shear, and Mixed Mode I/II) for a carbon-fiber epoxy composite (Fig. 7 right). Please note that Fig. 7 shows Paris-type graphs of da/dN versus G_{max} for the respective FRP composites and Modes.

In view of the effects of fiber-bridging discussed above, it could be hypothesized that the Mode I fatigue fracture data for AS4/PEEK (Fig. 7 left) would significantly change position and/or slope in the graph, if the test was run, e.g., using the procedure proposed in [41,75], and the data extrapolated to zero fiber bridging. It can, at this stage, however, not be excluded that Mode II would prove to be more conservative than Mode I for this carbon-fiber thermoplastic matrix composite material even after accounting for fiber bridging. So far (to the best knowledge of the author), there are no published

data for other carbon-fiber thermoplastic composites (e.g., PPS, or PES) under cyclic fatigue Mode II for comparison with cyclic fatigue Mode I.

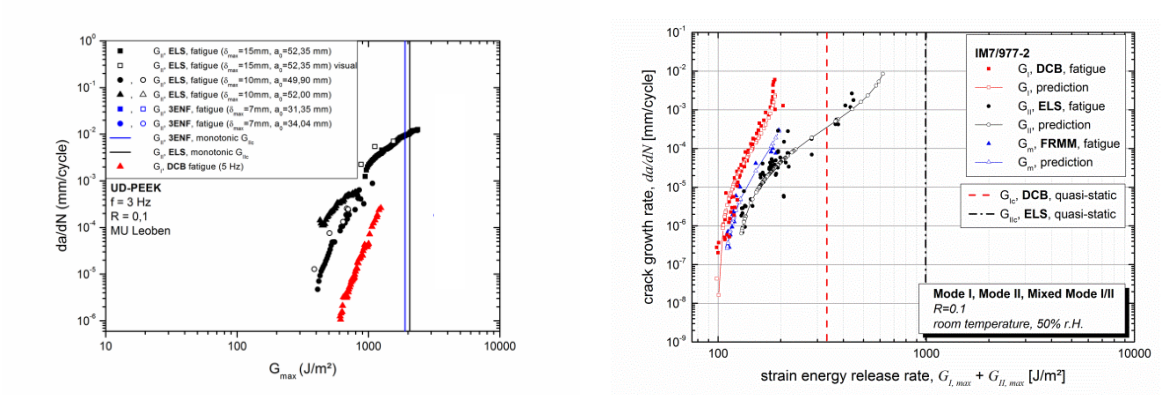

Figure 7: Paris-type graphs of (left) unidirectional AS4/PEEK carbon-fiber thermoplastic composite tested under Mode I and Mode II quasi-static and cyclic fatigue fracture, the quasi-static results are represented by the vertical lines, the cyclic fracture with open and closed symbols according to the insert, (right) the same plot for IM7/977-2 carbon-fiber duromer composite includes also Fixed-Ratio Mixed Mode I/II data (see text for details and discussion).

Fig. 7 right indicates that at low values of G_{max} the data for the different modes (Mode I, Mode II, here with a fixed ratio of 4:3 for Mixed Mode I/II, the blue line is the prediction for this ratio from the fitted Mode I and Mode II data) seem to converge near a value of 100 J/m^2 for low values of da/dN. It is not clear whether this is partly or fully due to limited measurement resolution, i.e. scatter, or representing the material behavior. Independent of this, it is likely that the threshold value for this material is 100 J/m^2 or less. If the Mode I data were determined without effects of fiber bridging, the resulting curves would likely be more conservative, i.e., move to the left in Fig. 7 or to the left and upward on the da/dN axis. This would result in an even lower (average) threshold value, unless the slope of the curve is changed significantly also by this. Therefore, the question whether FRP structural designs can be based on finite threshold values and their associated scatter (e.g., estimated by a given multiple of the standard deviation), or whether damage-tolerant designs (including appropriate non-destructive inspections) will be required for future safe operation of such structures, remains open. Both paths will require further research based on the basics outlined in this paper.

Acknowledgments
The contributions of Ms Đurđija Džodan (Empa, Mechanical Systems Engineering) and Mrs Anja Huch (Empa, Applied Wood Materials) for manufacturing, testing and analyzing the single-fiber tensile specimens, of Dr Gaurav Mohanty (Empa, Mechanics of Materials & Nanostructures) for the in-situ fiber push-in tests, Dr Rolf Kaufmann, Dr. Selina Kolokytha, and Mr Jürgen Hofmann (Empa, Center for X-ray Analytics) for the X-ray Computed Tomography and the 2D Fourier Transform analysis of the X-ray image slices of CFRP specimens after fracture tests as well as data analysis and graphical presentation by Dr. Steffen Stelzer (Montanuniversität Leoben) and extensive discussions of various aspects of fracture and fatigue fracture testing of FRP composites with Prof. René Alderliesten (Technical University Delft), Prof. Leslie Banks Sills and Dr. Ido Simon (Tel Aviv University), Prof. Alfredo de Morais (University of Aveiro), Prof. Rhys Jones (Monash University), Prof. Anthony J. Kinloch (Imperial College), and Prof. Markus G.R. Sause (Augsburg University) are gratefully acknolwedged.

References

[1] Paris PC, Gomez MP, Anderson WE 1961 *The Trend in Engineering* **13** 9-14.
[2] ASTM Standard E647 2015^{e1}, Measurement of Fatigue Crack Growth Rates, ASTM International, West Conshohocken, PA 1-49.
[3] Bathias C, Laksimi A 1985 *ASTM STP* **876** Delamination and Debonding of Materials, Johnson WS Ed. 217-237.
[4] Adams DF, Zimmerman RS, Odom EM 1987 *ASTM STP* **937** Toughened Composites, Johnston NJ Ed. 242-259.
[5] Hojo M, Gustafson CG, Tanaka K, Hayashi R 1987 *Compos. Sci. Technol.* **29** 273-292.
[6] O'Brien TK 1988 *J. Reinf. Plastics Compos.* **7** 341-359.
[7] Mall S, Yun KT, Kochhar NK 1989 *ASTM STP* **1012** Composite Materials: Fatigue and Fracture, Lagace PA Ed. 296-310.
[8] Newaz GM, Lustiger A, Yung JY 1989 *ASTM STP* **1044** Advances in Thermoplastic Matrix Composite Materials, Newaz GM Ed. 264-278.
[9] Hartman A, Schijve J 1970 *Eng. Fract. Mech.* **1** 615-631.
[10] Beden SM, Abdullah S,Ariffin AK, Al-Asady NA 2010 *Materials and Design* **31** 3449–3456.
[11] Sander M, Richard HA 2003 *Int. J. Fat.* **25** 999–1005.
[12] Zhang W, Wang Q, Li XY, He JJ 2016 *Mathematical Problems in Engineering* **2016** Article ID 4298507 1-8
[13] Maierhofer J, Pippan R, Gänser HP 2014 *Int. J. Fat.* **59** 200–207.
[14] Jones R, Pitt S, Brunner AJ, Hui D 2012 *Compos. Structs.* **94** 1343-1351.
[15] Jones R, Stelzer S, Brunner AJ 2014 *Compos. Structs.* **110** 317-324.
[16] Jones R, Kinloch AJ, Michopoulos JG, Brunner AJ, Phan N 2017 *Compos. Structs.* **180** 316-333
[17] Molent L, Forrester C 2017 *Compos. Structs.* **166** 22–26.
[18] Jones R. Raman, RKS, McMillan AJ 2018 *Eng. Fract. Mech.* **187** 190-210.
[19] Alderliesten RC, Brunner AJ, Pascoe JA 2018 submitted to *Eng. Fract. Mech.*
[20] ASTM D6115 1997 (reapproved 2011) Mode I Fatigue Delamination Growth Onset of Unidirectional Fiber-Reinforced Polymer Matrix Composites, ASTM International, West Conshohocken, PA 1-7.
[21] ASTM D5528 2013 Mode I Interlaminar Fracture Toughness of Unidirectional Fiber-Reinforced Polymer Matrix Composites, ASTM International, West Conshohocken, PA 1-13.
[22] Composites Materials Handbook CMH-17-3G 2017 **3** Materials Usage, Design and Analysis, Society of Automotive Engineers SAE.
[23] Composites Materials Handbook MIL-HDBK-17-3F 2002 **3** Polymer Matrix Composites Materials Usage, Design and Analysis.
[24] Davies P, Brunner AJ, Blackman BRK 1998 *Appl. Compos. Mats.* **5** 345-364.
[25] Tay TE 2003 *Appl. Mech. Rev.* **56** 1-31.
[26] Brunner AJ, Blackman BRK, Davies P 2008 *Eng. Fract. Mech.* **75** 2779-2794.
[27] Brunner AJ 2015 Chapt. 8 in *Polymer Composites in the Aerospace Industry*, Irving PE, Soutis C Eds, Woodhead Publishing, Series in Composites Science and Engineering **50** 191-230.
[28] JIS K7086 1993 Testing methods for interlarminar fracture toughness of carbon fibre reinforced plastics, Japanese Standards Association, Tokyo, 1-35.
[29] ISO 15024 2001 Fibre-reinforced plastic composites - Determination of mode I interlaminar fracture toughness, G_{IC}, for unidirectionally reinforced materials, International Organization for Standardization ISO, Geneva 1-24.
[30] ISO 15114 2014 Fibre-reinforced plastic composites - Determination of the mode II fracture resistance for unidirectionally reinforced materials using the calibrated end-loaded split (C-ELS) test and an effective crack length approach, International Organization for Standardization ISO, Geneva 1-18.
[31] ASTM D7905 2014 Determination of the Mode II Interlaminar Fracture Toughness of

Unidirectional Fiber-Reinforced Polymer Matrix Composites, ASTM International, West Conshohocken, PA 1-18.
[32] ASTM D6671/D6671M 2013^{e1} Mixed Mode I-Mode II Interlaminar Fracture Toughness of Unidirectional Fiber Reinforced Polymer Matrix Composites, ASTM International, West Conshohocken, PA 1-15.
[33] Murri G 2013 NASA-TM-2013-217996 Evaluation of Delamination Onset and Growth Characterization Methods under Mode I Fatigue Loading, Langley Research Center, Hampton VA 1-32.
[34] Stelzer S, Jones R, Brunner AJ 2013 Proc. 19th International Conference on Composites ICCM-19 Hoa SV, Hubert P Eds. Canadian Association for Composite Structures and Materials, Association Canadienne pour les Structures et Matériaux Composites, 1689-1697.
[35] Vinciquerra AJ, Davidson BD, Schaff JR, Smith SL 2002 *J. Reinf. Plastics Compos.* **217** 663-677.
[36] Brunner AJ, S. Stelzer S, G. Pinter G, Terrasi GP 2013 *Int. J. Fat.* **50** 57-62.
[37] Stelzer S, Brunner AJ, Pinter G 2015 Proc. 20th International Conference on Composite Materials ICCM-20, Paper-ID 3216-4, 1-7.
[38] Jaeck I, L. Carreras L, Renart J, Turon A, Martin de la Escalera F, Essa Y 2018 *Int. J. Fat.* **110** 63–70.
[39] Stelzer S, Brunner AJ, Argüelles A, Murphy N, Pinter G 2012 *Compos. Sci. Technol.* **72** 1102-1107.
[40] Stelzer S, Brunner AJ, Argüelles A, Murphy N, Cano GM, Pinter G 2014 *Eng. Fract. Mech.* **116**, 92-107.
[41] Yao LJ, Alderliesten RC, Jones R, Kinloch AJ 2018 *Compos. Structs.* **196** 8–20.
[42] Brunner AJ, Mujtaba A, Stelzer S, Jones R 2016 *Proc. Struct. Integ.* **2** 088-095.
[43] Gustafson CG, Hojo M 1987 *J. Reinf. Plastics Compos.* **6** 36-52.
[44] Rans C, Alderliesten R, Benedictus R 2011 *Compos. Sci. Technol.* **71** 230–238.
[45] Alderliesten RC 2013 *Eng. Fail. Anal.* **35** 370-379.
[46] Martin RH 2000 *Proc. Instn. Mech. Engrs. Part L* **214** 91-97.
[47] Murri GB 2006 *Int. J. Fat.* **28** 1124–1135.
[48] Murri GB, Schaff JR 2006 *Compos. Sci. Technol.* **66** 499–508.
[49] Cantwell WJ, Kausch HH 1993 *Mech. Compos. Mats.* **28** 328-333.
[50] Cantwell WJ 1996 *J. Mater.Sci. Lett.* **15** 639-641.
[51] Murri GB 2014 *J. Compos. Mats.* **48** 2413-2424.
[52] Blackman BRK, Brunner AJ, Williams JG 2006 *Eng. Fract. Mech.* **73** 2443–2455.
[53] Paruchuru SP, Kumar VU, Jain A, Dong XN 2017 *J. Test. Eval.* **45** 1139-1149.
[54] Hietschold N, Reinhardt R, Gurtner S 2014 *International Journal of Production Research* **52** 6254-6272.
[55] Davies P 1996 *Appl. Compos. Mats.* **3** 135-140.
[56] Brunner AJ, Tanner S, Davies P, Wittich H 1994 Proc. 2nd ECCM Conference on Composites Testing and Standardization ECCM-CTS 2, Hogg PJ, Schulte K, Wittich K Eds. Woodhead Publishing 523-532.
[57] de Moura MFSF, Morais JJL, Dourado N 2008 *Eng. Fract. Mech.* **75** 3852–3865.Ray BC, Hasan ST, Clegg DW 2007 *J. Reinf. Plast. Comp.* **26** 1187-1192.
[58] Ray BC, Hasan ST, Clegg DW 2007 *J. Reinf. Plast. Comp.* **26** 1187-1192.
[59] -Hsiao KT, Heider D 2017 Chapt. 10 in Manufacturing Techniques for Polymer Matrix Composites (PMCs), S.G. Advani AG, K.-T. Hsiao KT Eds. Woodhead Publishing 310-347.
[60] Yurgartis SW 1987 *Compos. Sci. Technol.* **30** 279-293.
[61] Makeev A, Seon G, Lee E 2010 *J. Compos. Mats.* **44** 95-112.
[62] Airoldi A, Dávila CG 2012 *Compos. Structs.* **94** 3240–3249.
[63] Manshadi BD, Farmand-Ashtiani E, Botsis J, Vassilopoulos AP 2014 *Compos.: Part A* **61** 43–50.

[64] Yao LJ, Sun Y, Guo LC, Jia LY, Zhao MY 2018 *Compos. Part B* **132** 97-106.
[65] Nicholls DJ, Gallagher JP 1983 *J. Reinf. Plast. Comp.* **2** 2-17.
[66] Sebaey TA, Blanco N, Costa J, Lopes, CS 2012 *Compos. Sci. Technol.* **72** 1251–1256.
[67] Chou I, Kimpara I, Kageyama K, Ohsawa I 1995 *ASTM STP* **1230** Composite Materials: Fatigue and Fracture--Fifth Volume, Martin RH Ed, American Society for Testing and Materials, Philadelphia, 132-151.
[68] Pelegri AA, Tekkam A 2003 *J. Compos. Mats.* **37** 579-596.
[69] Polaha JJ, Davidson BD, Hudson RC, Pieracci A. *J. Reinf. Plastics Compos.* **15** 141–173.
[70] Tao JX, Sun CT 1998 *J. Compos. Mats.* **32** 1933-1947.
[71] Shi YB, Hull D, Price JN 1993 *Compos. Sci. Technol.* **47** 173-184.
[72] Brunner AJ, Flüeler P 2005 *Eng. Fract. Mech.* **72** 899-908.
[73] Brunner AJ 2008 Chapt. 9 in *Delamination Behaviour of Composites*, Sridharan S Ed. Woodhead Publishing, Series in Composites Science and Engineering **25** 281-309.
[74] Choi NS, Kinloch AJ, Williams JG 1999 *J. Compos. Mats.* **33** 73-100.
[75] Yao LJ, Sun Y, Guo LC, Zhao MY, Jia LY, Alderliesten RC, Benedictus R 2017 *Compos. Structs.* **176** 556–564.
[76] Yao LJ, Sun Y, Guo LC, Lyu XQ, Zhao MY, Jia LY, Alderliesten RC, Benedictus R 2018 *Eng. Fract. Mech.* **189** 221–231.
[77] Alderliesten RC 2018 Proc. 39th Risø International Symposium on Materials Science 1-14.
[78] Hojo M, Ochiai S, Aoki T, Ito H 1994 Proc. 2nd ECCM Conference on Composites Testing and Standardization ECCM-CTS 2, Hogg PJ, Schulte K, Wittich K Eds. Woodhead Publishing 553-561.
[79] Hojo M, Aoki T 2015 Proc. 20th International Conference on Composite Materials ICCM-20 Paper-ID 2116-1 1-8.
[80] de Morais AB 2015 *J. Compos. Mats.* **49** 1681–1688.
[81] Sause MGR, Horn S 2010 J. Nondestruct. Eval. **29** 123–142.
[82] Bohse J 2000 *Compos. Sci. Technol.* **60** 1213-1226.
[83] Brunner AJ 2016 *J. Acoustic Emission* **33** S41-S46.
[84] Sause MGR, Gribov A, Unwin AR, Horn S 2012 *Pattern Recogn. Lett.* **33** 17–23.
[85] Sause MGR, Müller T, Horoschenkoff TA, Horn S 2012 *Compos. Sci. Technol.* **72** 167–174.
[86] Schubert L, Schulze E, Frankenstein B. 2011 Proc. 8th International Conference on Structural Dynamics, EURODYN 2011, De Roeck G, Degrande G, Lombaert G, Müller G. Eds. 3462-3468.
[87] Brunner AJ 2018 *Constr. Build. Mats.* **173** 629-637.
[88] Nordstrom RA 1995 ETH Zürich Ph.D. Thesis **11402** 1-168.
[89] Battisti A, Esqué-de los Ojos D, Ghisleni R, Brunner AJ 2014 *Compos. Sci. Technol.* **95** 121-127.
[90] Suzuki H, Takemoto M, Ono K 1987 *J. Acoust. Emiss.* **14** 35-50.
[91] Crasto AS, Corey R, J. T. Dickinson JT, Subramanian RV, Eckstein Y 1987 *Compos. Sci. Technol.* **30** 35-58.
[92] Dikshit V, Bhudolia SK, Joshi SC 2017 Fibers **2017 5, 38** 1-27.
[93] Martin RH, Murri GB 1990 *ASTM STP* **1059** Composite Materials: Testing and Design (Ninth Volume), Garbo SP Ed. American Society for Testing and Materials, Philadelphia 251-270.